JOURNAL OF GUIDANCE, CONTROL, AND DYNAMICS
Vol. 28, No. 4, July–August 2005

Velocity-Free Attitude Controllers Subject to Actuator Magnitude and Rate Saturations

Maruthi R. Akella* and Agustin Valdivia†
University of Texas at Austin, Austin, Texas 78712
and
Gnana R. Kotamraju‡
Microstrategy, Inc., McLean, Virginia 22102

We consider the "velocity-free" feedback control problem associated with attitude tracking for a rigid body subject to torque-magnitude and rate-saturation limits. Whereas no angular rate measurements are utilized within the feedback structure, the controller rigorously enforces actuator-magnitude and rate-saturation constraints. The associated stability proof is constructive and accomplished by the development of a novel Lyapunov function candidate. Although control smoothness is preserved at all times, it is important to note that the results of this paper that are derived with respect to magnitude saturation place no additional restrictions on the body inertias and make no other small-angle assumptions. The closed-loop performance of the new control solution derived here is evaluated extensively through numerical simulations in which we also include realistic levels of sensor noise in the feedback signals.

I. Introduction

THE rigid-body attitude control problem has been extensively investigated for many years due to its relevance to spacecraft attitude maneuvers, underwater vehicles and several other applications in robot manipulation. Full state-feedback solutions for these classes of problems that utilize both attitude and angular-velocity measurements can now be considered to be fully understood and solved (for example, Refs. 1–5). However, the assumption of availability of the angular-velocity measurement for use within the feedback signal is not always satisfied, because of either cost limitations or implementation considerations.

As a remedy to such situations, several important recent results have utilized passivity-based attitude-control strategies to guarantee global asymptotic stability when the feedback control signal is desired to be angular-velocity-free.[6–9] The underlying approach within all of these results is the construction of a dynamic filter driven by the attitude variable (say, the vector part of the quaternion[6,8] or the modified Rodrigues parameter vector[7,9]). These solutions provide the dual benefits not only of avoiding numerical differentiation of noise-corrupted attitude signals (dirty derivatives), but also of the assurance of a rigorous stability analysis.

Besides the obvious interest in ensuring closed-loop stability with bounded control torques, there is a practical motivation in introducing control and control-rate saturations nested into the loop. Dirty-derivative filters[10] and other approaches proposed in Ref. 11 have traditionally been adopted for output feedback stabilization of general nonlinear systems with saturated inputs. One of the first studies on the role of saturation constraints in the design of feedback controllers for mechanical systems was performed by Schaub and Junkins (see Ref. 12) using full-state feedback. This result was based on the kinematic work–energy principle but does not guarantee global asymptotic stability. Some recent results are also available within the robotics literature concerning Euler–Lagrange systems as seen in Loria and Nijmeijer[13] and references therein. These results adopt hyperbolic trignometric functions to provide semiglobal asymptotic stability with bounded (saturated) control inputs.

Nevertheless, all of the above-mentioned results hold only for the robotics problem, and as far as we know, the problem of output feedback attitude-tracking control for a rigid body with bounded inputs and bounded input rates remains open. In this paper, we tackle this problem by using a linear filter in a spirit similar to the recently proposed velocity-free attitude-tracking controller for rigid-body rotational motion.[9] However, in this study, the main complication arises from the fact that the inputs and the input rates are upper-bounded by a priori fixed constants. We show that by adoption of the once redundant unit-quaternion attitude representation in conjunction with the passivity-based filter construction and novel use of hyperbolic trignometric functions, this difficulty can be overcome. As will be seen in the following developments, compared to nonredundant three-parameter kinematic representations, direct parameterization of the overall attitude error by the four-dimensional quaternion vector is one of the crucial contributing factors behind our stability results.

The paper is organized as follows: in the following section, we provide a formal problem statement accompanied by all the governing equations. In Sec. III, we propose and output feedback control scheme and provide the associated stability analysis for the resulting closed-loop dynamics. Section IV presents numerical simulation results, and the paper is closed with some concluding remarks.

Notation: We use $\|\cdot\|$ for the Euclidean norm of vectors and the induced norm of matrices. We denote $\mathrm{Tanh}\,\boldsymbol{q} \doteq \mathrm{col}[\tanh(q_1), \ldots, \tanh(q_n)]$ for all $\boldsymbol{q} = \mathrm{col}[q_1, \ldots, q_n] \in \mathcal{R}^n$. The set of n times continuously differentiable functions is denoted by $\mathcal{C}^n$. The largest and smallest eigenvalues of any real symmetric and positive definite matrix K are denoted by k_M and k_m respectively. Finally, we adopt $\dot{\boldsymbol{q}}(t)$ to denote the time derivatives of both vector and matrix functions $\boldsymbol{q}(t)$.

II. Problem Formulation

A. Governing Equations

The rotational motion of a rigid body is described by the well-known Euler equation, represented by

$$I\dot{\omega} = -S(\omega)I\omega + \boldsymbol{u} \tag{1}$$

Received 4 March 2004; revision received 1 June 2004; accepted for publication 1 June 2004.

*Assistant Professor, Department of Aerospace Engineering and Engineering Mechanics; makella@mail.utexas.edu. Member AIAA.

†Graduate Research Assistant, Department of Aerospace Engineering and Engineering Mechanics.

‡Senior Quality Engineer, 1861 International Drive; gkotamraju@microstrategy.com.

where $\omega(t) \in \mathcal{R}^3$ is the angular velocity given in a body-fixed frame of reference, $I = I^T \in \mathcal{R}^{3\times 3}$ is the positive-definite mass-moment-of-inertia matrix, and $\boldsymbol{u}(t) \in \mathcal{R}^3$ is an external torque input vector that is subject to both magnitude and rate constraints given by

$$\|\boldsymbol{u}(t)\| \le u_{\mathrm{m}} \qquad \text{and} \qquad \|\dot{\boldsymbol{u}}(t)\| \le \dot{u}_{\mathrm{m}} \tag{2}$$

for all $t \in \mathcal{R}$. Also, in Eq. (1), $S(\cdot)$ denotes the skew-symmetric matrix operator that performs the vector cross product in such a way that $S(\boldsymbol{a})\boldsymbol{b} = \boldsymbol{a} \times \boldsymbol{b}$ for every $\boldsymbol{a}, \boldsymbol{b} \in \mathcal{R}^3$.

As far as the kinematics is concerned, we adopt the unit quaternion vector $\boldsymbol{\beta}(t) \in \mathcal{R}^4$ to designate the attitude of the rigid body relative to any target attitude. This is the minimal representation of the rigid-body kinematics that is globally nonsingular. Moreover, as we will show in the subsequent developments, the quaternion parameterization, which is subject to the constraint $\|\boldsymbol{\beta}(t)\| = 1$ for all $t \in \mathcal{R}$, is beneficial from the point of view of imposing control saturation constraints and ensuring smoothness of the control inputs.

The unit-quaternion representation of the rotation matrix is defined by the equations

$$\boldsymbol{\beta} = [\beta_0, \beta_1, \beta_2, \beta_3]^T = [\beta_0, \boldsymbol{\beta}_v]^T, \qquad \beta_0 = \cos(\phi/2);$$
$$\boldsymbol{\beta}_v = \boldsymbol{k}\sin(\phi/2) \tag{3}$$

where ϕ is the corresponding rotation angle about the Euler principal rotation axis $\boldsymbol{k}$. The rotation matrix C is related to the quaternion $\boldsymbol{\beta}$ through

$$C(\boldsymbol{\beta}) = I + 2\beta_0 S(\boldsymbol{\beta}_v) + 2S^2(\boldsymbol{\beta}_v) \tag{4}$$

Given the 3×3 proper orthogonal matrix C, the vector $\boldsymbol{\beta}$ can be computed from Stanley's algorithm.[14] It should be noted that both vectors $+\boldsymbol{\beta}$ and $-\boldsymbol{\beta}$ represent the same rotation matrix C. However, this sign ambiguity does not cause any problems because it can always be resolved from the kinematic differential equations given by

$$\dot{\boldsymbol{\beta}} = \tfrac{1}{2}E(\boldsymbol{\beta})\boldsymbol{\omega} \tag{5}$$

where the matrix $E = E(\boldsymbol{\beta})$ is given by[6,15]

$$E(\boldsymbol{\beta}) = \begin{bmatrix} -\boldsymbol{\beta}_v^T \\ \beta_0 I_{3\times 3} - S(\boldsymbol{\beta}_v) \end{bmatrix} \tag{6}$$

with $I_{3\times 3}$ being the 3×3 identity matrix. It can easily be verified from the preceding definition that

$$E^T(\boldsymbol{\beta})E(\boldsymbol{\beta}) = I_{3\times 3}, \qquad E^T(\boldsymbol{\beta})\boldsymbol{\beta} = \boldsymbol{0} \tag{7}$$

Consequent to Eq. (5), the angular velocity vector can be expressed in terms of $\boldsymbol{\beta}$ and $\dot{\boldsymbol{\beta}}$ as

$$\boldsymbol{\omega} = 2E^T(\boldsymbol{\beta})\dot{\boldsymbol{\beta}} \tag{8}$$

Thus, we adopt Eqs. (1) and (5) to govern the nonlinear dynamics of rigid-body rotational motion over the seven-dimensional $[\boldsymbol{\beta}, \boldsymbol{\omega}]^T$ space subject to the unit norm constraint on $\boldsymbol{\beta}$.

B. Reference Trajectory and Tracking Errors

To track commanded attitude motions, various reference frames need to be introduced. Let N be the inertial frame and let B be a body-fixed frame. The reference frame corresponding to the commanded motion is denoted by R. We choose to denote the commanded reference trajectory in terms of the reference quaternion vector $\boldsymbol{\beta}_c$, the commanded angular velocity $\boldsymbol{\omega}_c$, and the angular acceleration $\dot{\boldsymbol{\omega}}_c$. Let $\hat{\boldsymbol{b}}$, $\hat{\boldsymbol{r}}$, and $\hat{\boldsymbol{n}}$ represent the unit-vector triads in the B, R, and N frames, respectively. Further, let quaternions $\boldsymbol{\beta}$, $\boldsymbol{\beta}^c$, and $\boldsymbol{e}$ parameterize the direction-cosine matrices correspondingly between various reference frames as follows [Note: $C(\boldsymbol{e}) = C(\boldsymbol{\beta})C^T(\boldsymbol{\beta}^c)$]:

$$\mathsf{N} \xrightarrow{\boldsymbol{\beta}} \mathsf{B} \Rightarrow \hat{\boldsymbol{b}} = C(\boldsymbol{\beta})\hat{\boldsymbol{n}}$$
$$\mathsf{N} \xrightarrow{\boldsymbol{\beta}^c} \mathsf{R} \Rightarrow \hat{\boldsymbol{r}} = C(\boldsymbol{\beta}^c)\hat{\boldsymbol{n}}$$
$$\mathsf{R} \xrightarrow{\boldsymbol{e}} \mathsf{B} \Rightarrow \hat{\boldsymbol{b}} = C(\boldsymbol{e})\,\hat{\boldsymbol{r}} \tag{9}$$

Definitions for direction-cosine matrices $C(\boldsymbol{\beta}^c)$ and $C(\boldsymbol{e})$ can be obtained by simply replacing $\boldsymbol{\beta}$ in Eq. (4) by $\boldsymbol{\beta}^c$ and $\boldsymbol{e}$, respectively. Given the direction-cosine matrices $C(\boldsymbol{\beta})$ and $C(\boldsymbol{\beta}^c)$, the error quaternion vector $\boldsymbol{e}$ can again be calculated via Stanley's algorithm from $C(\boldsymbol{e}) = C(\boldsymbol{\beta})C^T(\boldsymbol{\beta}^c)$.

The quaternion vector $\boldsymbol{e}$ is a direct parameterization of the attitude error. On the other hand, the angular-velocity error vector $\boldsymbol{\delta\omega}$ can be obtained as the difference between the body velocity $\boldsymbol{\omega}$ and the commanded angular velocity $\boldsymbol{\omega}_c$. Extra caution is required in computing $\boldsymbol{\delta\omega}$ because most often it is natural to assign the commanded angular velocity $\boldsymbol{\omega}_c$ (and also the commanded acceleration $\dot{\boldsymbol{\omega}}_c$) with respect to the reference frame R. In such a case, the direction cosine matrix $C(\boldsymbol{e})$ can be used to map the R frame components of $\boldsymbol{\omega}_c$ into B frame components using the transformation

$$\boldsymbol{\omega}_c^{\mathsf{B}} = C(\boldsymbol{e})\,\boldsymbol{\omega}_c \tag{10}$$

The angular-velocity error $\boldsymbol{\delta\omega}$ may now be obtained using the formula

$$\boldsymbol{\delta\omega} = \boldsymbol{\omega} - \boldsymbol{\omega}_c^{\mathsf{B}} \tag{11}$$

However, computation of the commanded acceleration vector $\dot{\boldsymbol{\omega}}_c^{\mathsf{B}}$ in the body frame B requires additional knowledge of the body angular velocity $\boldsymbol{\omega}$ via the equality

$$\dot{\boldsymbol{\omega}}_c^{\mathsf{B}} = C(\boldsymbol{e})\dot{\boldsymbol{\omega}}_c - S(\boldsymbol{\omega})\boldsymbol{\omega}_c^{\mathsf{B}} = C(\boldsymbol{e})\dot{\boldsymbol{\omega}}_c - S(\boldsymbol{\omega})C(\boldsymbol{e})\boldsymbol{\omega}_c \tag{12}$$

It is reasonable to assume that the quantities $\boldsymbol{\omega}_c(t)$ and $\dot{\boldsymbol{\omega}}_c(t)$ and the higher derivatives of $\dot{\boldsymbol{\omega}}_c(t)$ are all uniformly bounded by finite positive values that are a priori available. In other words, for all $t \ge 0$, they satisfy

$$\|\boldsymbol{\omega}_c(t)\| \le \omega_{\mathrm{cm}}, \qquad \|\dot{\boldsymbol{\omega}}_c(t)\| \le \dot{\omega}_{\mathrm{cm}}, \qquad \text{and} \qquad \|\ddot{\boldsymbol{\omega}}_c(t)\| \le \ddot{\omega}_{\mathrm{cm}}$$

Now, we can state the governing differential equations for attitude error vector $\boldsymbol{e}$ and angular-velocity error $\boldsymbol{\delta\omega}$ as follows:

$$\dot{\boldsymbol{e}} = \tfrac{1}{2}E(\boldsymbol{e})\boldsymbol{\delta\omega} \tag{13}$$

$$I\dot{\boldsymbol{\delta\omega}} = -S(\boldsymbol{\omega})I\boldsymbol{\omega} + \boldsymbol{u} - I[C(\boldsymbol{e})\dot{\boldsymbol{\omega}}_c - S(\boldsymbol{\omega})C(\boldsymbol{e})\boldsymbol{\omega}_c] \tag{14}$$

where Eq. (14) is obtained by combining Eq. (1) with Eqs. (11) and (12). Thus, the control objective would be to determine the vector $\boldsymbol{u}$ subject to bounds specified by Eq. (2) such that the closed-loop trajectories described by Eqs. (13) and (14) are stable and they converge to the set $\Omega = \{e_0 = \pm 1, \boldsymbol{e}_v = \boldsymbol{0}, \boldsymbol{\delta\omega} = \boldsymbol{0}\}$.

III. Velocity-Free Control Solution with Actuator-Magnitude and Rate Constraints

In this section, we show that tracking errors $\boldsymbol{e}$ and $\boldsymbol{\delta\omega}$ governed by Eqs. (13) and (14) can be controlled without angular-velocity $\boldsymbol{\omega}$ feedback and, thus, only orientation $\boldsymbol{\beta}$ feedback is required. The attitude error vector $\boldsymbol{e}$ can be computed from the values of $\boldsymbol{\beta}$ and $\boldsymbol{\beta}^c$ by making use of identities in Eqs. (4) and (9). In the following theorem, we summarize our control solution to the underlying output feedback attitude-tracking problem subject to the actuator-magnitude and rate constraints stated in Eq. (2).

Theorem 1: Consider the system governed by Eqs. (13) and (14) and assume that there exist strictly positive scalar constants k_p, k_z, and λ that satisfy the inequalities

$$\text{A1)} \qquad u_m \geq k_p + k_z + I_M\left(\dot{\omega}_{\text{cm}} + \omega_{\text{cm}}^2\right) \tag{15}$$

$$\text{A2)} \qquad \dot{u}_m \geq \left[k_p/2 + k_z\left(1 + \lambda/2\sqrt{3}\right) + I_M\left(\dot{\omega}_{\text{cm}} + 2\omega_{\text{cm}}^2\right)\right] \times \sqrt{2V_0/I_m} + 2k_z k^2\lambda/\sqrt{3} + I_M(\ddot{\omega}_{\text{cm}} + 2\omega_{\text{cm}}\dot{\omega}_{\text{cm}}) \tag{16}$$

where the constant V_0 is defined by

$$V_0 = \tfrac{1}{2} I_M m_{\delta\omega}^2 + 4k_p \qquad \text{for any} \qquad m_{\delta\omega} > \|\boldsymbol{\delta\omega}(0)\| \tag{17}$$

Let the filter vector $\boldsymbol{z}(t) \in \mathcal{R}^3$ be generated as the solution of the linear differential equation

$$\dot{\boldsymbol{z}}(t) = \boldsymbol{e}_v - k^2\boldsymbol{z}, \qquad \text{with} \qquad \boldsymbol{z}(0) = (1/k^2)\boldsymbol{e}_v(0) \qquad \text{for some} \qquad k \in \mathcal{R} \tag{18}$$

Then the control input

$$\boldsymbol{u}(t) = -k_p\boldsymbol{e}_v - \left(k_z/\sqrt{3}\right)[e_0 I_{3\times 3} + S(\boldsymbol{e}_v)]\,\text{Tanh}\left(\lambda\left(\boldsymbol{e}_v - k^2\boldsymbol{z}\right)\right) + IC(\boldsymbol{e})\dot{\boldsymbol{\omega}}_c + S\left(\boldsymbol{\omega}_c^{\mathsf{B}}\right)I\boldsymbol{\omega}_c^{\mathsf{B}} \tag{19}$$

satisfies the control constraints in Eq. (2). At the same time, all the trajectories of the resulting closed-loop system are guaranteed to be bounded for all $t \geq 0$ and, furthermore, they asymptotically converge to the set defined by $\Omega = \{e_0 = \pm 1, \boldsymbol{e}_v = \boldsymbol{0}, \boldsymbol{\delta\omega} = \boldsymbol{0}\}$.

Before we proceed with the proof for Theorem 1, the following remarks are in order:

Remark 1: Assumption (A1) in Eq. (15) is due to the control-magnitude constraint and likewise, assumption (A2) in Eq. (16) is due to the actuator-rate constraint. In the absence of the magnitude and rate constraints, one is free to select any finite and strictly positive value for the control gains k_p and k_z within the control torque expression given by Eq. (19).

Remark 2: The control-rate constraint (A2) in Eq. (16) depends on the quantity V_0, which in turn depends on the initial angular velocity $\boldsymbol{\omega}(0)$ (more specifically, $\|\boldsymbol{\delta\omega}(0)\| \leq m_{\delta\omega}$), as can be seen from Eq. (17). Thus, whereas the control solution is "velocity-free," one does require at least an estimated upper bound on the initial body angular-rate errors to satisfy the control-rate saturation constraint. In the case in which only the control-magnitude constraint is of interest, the gain variables k_p and k_z can be selected, taking only Eq. (15) into consideration, thereby obviating the need for knowledge of an upper bound on the norm of the initial angular-velocity error vector. By the same argument, one can further observe that global asymptotic stability for the tracking errors can be ensured by the control law in Eq. (19) when only the actuator-magnitude saturation constraint is of interest.

Remark 3: In the attitude-regulation special case, the quantities ω_{cm}, $\dot{\omega}_{\text{cm}}$, and $\ddot{\omega}_{\text{cm}}$ in Eqs. (15) and (16) can all be as taken equal to zero and, thus, we may rewrite the two assumptions within the statement of Theorem 1 as follows:

$$\text{A1}') \qquad u_m \geq k_p + k_z \tag{20}$$

$$\text{A2}') \quad \dot{u}_m \geq \left[k_p/2 + k_z\left(1 + \lambda/2\sqrt{3}\right)\right]\sqrt{2V_0/I_m} + 2k_z k^2\lambda/\sqrt{3} \tag{21}$$

Notice from Eq. (20) that the modified control-magnitude constraint (A1)′ no longer requires any information on the largest eigenvalue of the inertia matrix I_M. In this context, it is important to note that the so-called reduction property[9] for attitude regulation (in the absence of any actuator constraints) ensures that global stabilization can be achieved without any knowledge whatsoever of the body inertia matrix. We observe from Eq. (20) that the same reduction property holds true even when one is interested in imposing only the actuator-magnitude-saturation condition. On the other hand, the control-rate-saturation condition Eq. (21) still requires information on the largest and smallest eigenvalues (I_M and I_m, respectively) of the inertia matrix (or at least their upper and lower bounds, respectively) along with the body initial-angular-velocity vector for the attitude-regulation special case.

Remark 4: The control torque $\boldsymbol{u}(t)$ defined in Eq. (19) is independent of the angular velocity and is hence termed velocity-free. It remains smooth for all bounded and smooth reference trajectories. Furthermore, in the case of set-point attitude regulation, the last two terms on the right-hand side of Eq. (19) drop out. The resulting control solution has a structure somewhat similar to the passivity-based control solution presented by Lizarralde and Wen[6] except for the significant difference due to the presence of new terms involving the hyperbolic trignometric functions. An important consequence is that for this special case of attitude regulation, the proposed controller does not require knowledge of the rigid body inertia parameters as long as the control gains k_p and k_z are in accordance with Eqs. (20) and (21) and is hence robust to inertia uncertainty.

Remark 5: When compared with existing results in the literature, the additional incorporation of the hyperbolic trignometric functions lends novelty to the control law stated by Eq. (19) of Theorem 1. It may be further observed that the tanh functions remain rigorously smooth and the time rate of their change (degree of smoothness) is a direct function of the parameter λ. All other things remaining the same, a larger value for λ ultimately leads to a higher magnitude for the time derivative of the control torque. In other words, the parameter λ provides an additional design knob within the control torque provided by Theorem 1 that could be gainfully adopted for improving the closed-loop performance. This aspect will be further illustrated through numerical simulation examples provided in the sequel.

Remark 6: The filter state $\boldsymbol{z}(t)$ satisfies the stable first-order linear vector differential equation defined in Eq. (18) that is driven by the forcing term $\boldsymbol{e}_v(t)$ and is nearly identical to the filter dynamics presented in earlier passivity-based output feedback control schemes.[6,7,9] In terms of frequency-response characteristics, these filter dynamics can therefore be viewed as a low-pass system for all bounded $\boldsymbol{e}_v(t)$ signals. The only notable difference compared to the existing passivity-based solutions of Refs. 6, 7, and 9 is the choice of the initial condition $\boldsymbol{z}(0) = \boldsymbol{e}_v(0)/k^2$. This selection not only ensures that $\|\boldsymbol{z}(t)\| \leq 1/k^2$ for all $t \geq 0$ but also provides a smaller value for V_0, as will be clear from the stability proof given in the sequel. The advantage is that given a control-rate saturation value $\dot{u}_m$, smaller value of V_0 ensures greater flexibility in obtaining feasible values for control gains k_p and k_z consistent with the inequalities in either Eq. (16) or Eq. (21). We should also point out that the value of filter gain k plays an important role in defining the low-pass characteristics of the filter state $\boldsymbol{z}$. The ultimate choice of this design parameter would indeed be dictated by signal noise levels encountered within practical applications.

Proof of Theorem 1: The proof uses elements of Lyapunov stability theory and is organized as follows. We first propose a Lyapunov function candidate that is globally decrescent and radially unbounded in the tracking errors; then we prove that the time derivative of this Lyapunov function is negative semidefinite along trajectories generated by Eqs. (13) and (14). Next, we invoke the uniform continuity type of argument associated with Barbalat's lemma to show that the closed-loop system is asymptotically stable in the sense of Theorem 1. We conclude the proof by showing that the control input $\boldsymbol{u}(t)$ defined in Eq. (19) indeed satisfies the magnitude and rate constraints defined in Eq. (2) as long as the feedback gains k_p and k_z are selected in accordance with assumptions (A1) and (A2).

Now, consider the following Lyapunov function candidate, which is inspired by a similar construction within the context of the Euler–Lagrange systems,[13]

$$V = \frac{1}{2}\boldsymbol{\delta\omega}^T I\,\boldsymbol{\delta\omega} + k_p\left[(e_0 - 1)^2 + \boldsymbol{e}_v^T\boldsymbol{e}_v\right] + \frac{2k_z}{\sqrt{3}\lambda}\sum_{i=1}^{3}\log\cosh\left[\lambda\left(\boldsymbol{e}_{vi} - k^2\boldsymbol{z}_i\right)\right] \tag{22}$$

which is positive definite and proper. Following tedious but fairly straightforward algebra, the time derivative of $V(t)$ evaluated along the closed-loop trajectories can be established as

$$\dot{V} = -\left(2k_z/\sqrt{3}\lambda\right)\left(\boldsymbol{e}_v - k^2\boldsymbol{z}\right)^T \tanh\left[\lambda\left(\boldsymbol{e}_v - k^2\boldsymbol{z}\right)\right]$$
$$= -\left(2k_z/\sqrt{3}\lambda\right)\dot{\boldsymbol{z}}^T \tanh(\lambda\dot{\boldsymbol{z}}) \leq 0 \tag{23}$$

Therefore, $\boldsymbol{\delta\omega}(t)$, $\boldsymbol{e}_v(t)$, $\boldsymbol{z}(t)$, and $\dot{\boldsymbol{z}}(t)$ are all uniformly bounded. Also, because $V \geq 0$ and $\dot{V} \leq 0$, we have that $\lim_{t\to\infty} V(t) \doteq V_\infty$ exists for some finite $V_\infty \in \mathcal{R}^+$. Also, from Eq. (23) and boundedness of all signals within subsequent time derivatives of $V(t)$, it is easy to establish that $\ddot{V}(t) \in \mathcal{L}_\infty$ or, in order words, uniform continuity for $\dot{V}(t)$. This result, in conjunction with the convergence of $V(t)$ to V_∞ permits application of Barbalat's lemma (using the alternate statement of this lemma from Ref. 16) to provide $\dot{V}(t) \to 0$ as $t \to \infty$. This lets us go further and conclude that $\lim_{t\to\infty} \dot{\boldsymbol{z}}(t) = 0$. Next, by virtue of the fact that the third time derivative of the function $\boldsymbol{z}(t)$ is uniformly bounded, we conclude uniform continuity for $\ddot{\boldsymbol{z}}(t)$. Also, because $\lim_{t\to\infty} \dot{\boldsymbol{z}}(t) = 0$, we also have

$$\lim_{t\to\infty} \int_0^t \ddot{\boldsymbol{z}}(\tau)\mathrm{d}\tau + \dot{\boldsymbol{z}}(0) = 0$$

which when interpreted together with the uniform continuity of $\ddot{\boldsymbol{z}}(t)$ permits reapplication of Barbalat's lemma and finally leads to $\lim_{t\to\infty} \ddot{\boldsymbol{z}}(t) = 0$. Again, because $\ddot{\boldsymbol{z}} = -k^2\dot{\boldsymbol{z}} + \dot{\boldsymbol{e}}_v$, it follows that $\dot{\boldsymbol{e}}_v(t) \to 0$ as $t \to \infty$. Now, starting with the unit norm constraint on the quaternion vector $e_0(t)^2 + \boldsymbol{e}_v^T(t)\boldsymbol{e}_v(t) = 1$, and differentiating both sides with respect to time, it follows that $\lim_{t\to\infty} e_0(t)\dot{e}_0(t) = 0$ after making use of $\lim_{t\to\infty} \dot{\boldsymbol{e}}_v(t) = 0$. Therefore we have the following cases: 1) $\lim_{t\to\infty} e_0(t) = 0$ and/or 2) $\lim_{t\to\infty} \dot{e}_0(t) = 0$. Let us initially assume that $\lim_{t\to\infty} e_0(t) = 0$ but $\lim_{t\to\infty} \dot{e}_0(t) \neq 0$. In this case, using boundedness of various signals on the right-hand sides of Eqs. (13) and (14), it is possible to conclude that $\ddot{e}_0(t)$ is bounded, thereby implying uniform continuity for $\dot{e}_0(t)$. Also,

$$\lim_{t\to\infty} e_0(t) = 0 = \lim_{t\to\infty} \int_0^t \dot{e}_0(\tau)\,\mathrm{d}\tau$$

and using Barbalat's lemma, we obtain $\lim_{t\to\infty} \dot{e}_0(t) = 0$, which contradicts our assumption that $\lim_{t\to\infty} \dot{e}_0(t) \neq 0$. Therefore, irrespective of whether it is case 1) or case 2), it always follows that $\lim_{t\to\infty} \dot{e}_0(t) = 0$. However, at this point, it still remains to be shown what happens to $e_0(t)$ as $t \to \infty$.

We proceed by using the facts that $\dot{\boldsymbol{e}}_v(t) = 0$ and $\dot{e}_0(t) = 0$ as $t \to \infty$, which means that the left-hand side of Eq. (13) equals zero. Premultiplying both sides of Eq. (13) by the matrix $E^T(\boldsymbol{e})$ and using the identity stated in Eq. (7), it follows that $\lim_{t\to\infty} \boldsymbol{\delta\omega}(t) = 0$. Next, Eq. (14) may be differentiated to show that $\ddot{\boldsymbol{\delta\omega}} \in \mathcal{L}_\infty$ which implies that $\dot{\boldsymbol{\delta\omega}}(t)$ is uniformly continuous or by applying Barbalat's lemma one more time, we have $\dot{\boldsymbol{\delta\omega}}(t) \to 0$ as $t \to \infty$. This last result, together with the control law given in Eq. (19), can be used in Eq. (14) to demonstrate that $-k_p\boldsymbol{e}_v(t) \to 0$ as $t \to \infty$. We therefore obtain $\lim_{t\to\infty} \|\boldsymbol{e}_v(t)\|^2 = 0$ or $\lim_{t\to\infty} \boldsymbol{e}_v(t) = 0$ and consequently from the unit-norm constraint on the unit-error quaternion, $\lim_{t\to\infty} e_0(t) \neq 0$ (more precisely, $\lim_{t\to\infty} e_0(t) = \pm 1$). Finally, because $\lim_{t\to\infty} \boldsymbol{e}_v(t) = 0$, from Eq. (18) we note that $\dot{\boldsymbol{z}}(t) + k^2\boldsymbol{z}(t) \to 0$ as $t \to \infty$ and therefore $\lim_{t\to\infty} \boldsymbol{z}(t) = 0$. Thus we are able to show that

$$\lim_{t\to\infty} [\boldsymbol{e}_v(t), \boldsymbol{\delta\omega}(t), \boldsymbol{z}(t)] = 0$$

thereby completing the proof of achieving the stated tracking objective.

We now proceed to show that the control torque in Eq. (19) satisfies the magnitude and rate conditions of Eq. (2) for all $t \geq 0$. Because $\boldsymbol{e}(t)$ corresponds to the attitude error quaternion, by definition, $\|\boldsymbol{e}_v(t)\| \leq 1$ and $|e_0(t)| \leq 1$. From Eq. (6) and Eq. (7), it follows that $\|e_o I_{3\times 3} + S(\boldsymbol{e}_v)\| \leq 1$. Further, from Eq. (18), it is straightforward to establish that $\|\boldsymbol{z}(t)\| \leq 1/k^2$ for all $t \geq 0$ as long as we select $\|\boldsymbol{z}(0)\| \leq 1/k^2$. Thus, making use of all the inequalities and upper bounds derived in the foregoing within Eq. (19), we have

$$\|\boldsymbol{u}\| \leq k_p + k_z + I_M\left[\|C(\boldsymbol{e})\|\|\dot{\boldsymbol{\omega}}_c\| + \left\|\boldsymbol{\omega}_c^{\mathcal{B}}\right\|^2\right] \tag{24}$$

Because $C(\boldsymbol{e})$ is a direction cosine matrix, $\|C(\boldsymbol{e})\|$ is always equal to unity and as a consequence, $\|\boldsymbol{\omega}_c^{\mathcal{B}}\| = \|\boldsymbol{\omega}_c\| \leq \omega_{\mathrm{cm}}$. Thus, an upper bound for $\boldsymbol{u}(t)$ can be obtained from Eq. (24) as follows:

$$\|\boldsymbol{u}\| \leq k_p + k_z + I_M\left(\dot{\omega}_{\mathrm{cm}} + \omega_{\mathrm{cm}}^2\right) \tag{25}$$

This inequality is obviously identical to assumption (A1) in Eq. (15) and, thus, we conclude that $\|\boldsymbol{u}(t)\| \leq u_m$ for all $t \geq 0$.

Finally, in order to demonstrate that $\boldsymbol{u}(t)$ satisfies the rate-saturation constraint in Eq. (2), we need to proceed with term-by-term differentiation of Eq. (19). Before we actually do that, we can make use of Eq. (7) within Eq. (13) to obtain $\|\dot{\boldsymbol{e}}_v\| \leq \|\boldsymbol{\delta\omega}\|/2$ and $|\dot{e}_0| \leq \|\boldsymbol{\delta\omega}\|/2$. Because $V(t) \leq V(0)$, from Eq. (23), we then use the definition of $V(t)$ in Eq. (22) to obtain $\|\boldsymbol{\delta\omega}\|^2 \leq 2V(t)/I_m \leq 2V(0)/I_m$. Moreover, from Eq. (17), if we note that $V(0) \leq V_0$, then we are led to the inequality

$$\|\dot{\boldsymbol{e}}_v(t)\| \leq \frac{1}{2}\|\boldsymbol{\delta\omega}(t)\| \leq \sqrt{\frac{V(t)}{2I_m}} \leq \sqrt{\frac{V(0)}{2I_m}} \leq \sqrt{\frac{V_0}{2I_m}}, \qquad \forall t \geq 0 \tag{26}$$

Notice that selecting $\boldsymbol{z}(0) = \boldsymbol{e}_v(0)/k^2$ essentially eliminates the term

$$\frac{2k_z}{\sqrt{3}\lambda}\sum_{i=1}^{3} \log\cosh\left[\lambda\left(\boldsymbol{e}_{vi} - k^2\boldsymbol{z}_i\right)\right]$$

within $V(t)$ in Eq. (22) when evaluated at $t = 0$. If this choice were not made (see Remark 6 stated earlier), then the upper bound V_0 on $V(0)$ would have to be appropriately modified in Eq. (17) by adding a nonzero positive quantity

$$\frac{2k_z}{\sqrt{3}\lambda}\sum_{i=1}^{3} \log\cosh\left[\lambda\left(\boldsymbol{e}_{vi}(0) - k^2\boldsymbol{z}_i(0)\right)\right]$$

Now, by proceeding with differentiation of Eq. (19) with respect to time, and making use of the signal upper bounds that we derived so far, it can be shown that

$$\|\dot{\boldsymbol{u}}(t)\| \leq \frac{2k_z k^2\lambda}{\sqrt{3}} + \left[\frac{k_p}{2} + k_z\left(1 + \frac{\lambda}{2\sqrt{3}}\right)\right]\|\boldsymbol{\delta\omega}(t)\|$$
$$+ \left\|\frac{\mathrm{d}}{\mathrm{d}t}\left[IC(\boldsymbol{e})\dot{\boldsymbol{\omega}}_c + S\left(\boldsymbol{\omega}_c^{\mathcal{B}}\right)I\boldsymbol{\omega}_c^{\mathcal{B}}\right]\right\| \tag{27}$$

Recalling the classical Poisson equation from rigid-body kinematics, the direction cosine matrix $C(\boldsymbol{e})$ satisfies the differential equation[17]

$$\frac{\mathrm{d}}{\mathrm{d}t}C(\boldsymbol{e}) = -S(\boldsymbol{\delta\omega})C(\boldsymbol{e})$$

We deduce that

$$\left\|\frac{\mathrm{d}}{\mathrm{d}t}C(\boldsymbol{e})\right\| \leq \|\delta\omega(t)\|$$

We can employ this inequality within the last term inside the parentheses on the right hand side of Eq. (27) to obtain

$$\|\dot{\boldsymbol{u}}(t)\| \leq 2k_z k^2\lambda/\sqrt{3} + \left[k_p/2 + k_z\left(1 + \lambda/2\sqrt{3}\right)\right]\|\boldsymbol{\delta\omega}(t)\|$$
$$+ I_M\left(\dot{\omega}_{\mathrm{cm}} + 2\omega_{\mathrm{cm}}^2\right)\|\boldsymbol{\delta\omega}(t)\| + I_M(\ddot{\omega}_{\mathrm{cm}} + 2\omega_{\mathrm{cm}}\dot{\omega}_{\mathrm{cm}}) \tag{28}$$

Substituting the upper bound on $\|\delta\boldsymbol{\omega}(t)\|$ in Eq. (26) and rearranging terms, we finally write

$$\|\dot{\boldsymbol{u}}(t)\| \le \left[k_p/2 + k_z\left(1 + \lambda/2\sqrt{3}\right) + I_M\left(\dot{\omega}_{\rm cm} + 2\omega_{\rm cm}^2\right)\right]\sqrt{2V_0/I_m} + 2k_z k^2\lambda/\sqrt{3} + I_M(\ddot{\omega}_{\rm cm} + 2\omega_{\rm cm}\dot{\omega}_{\rm cm}) \tag{29}$$

which is again identically the same condition expressed in the control-rate saturation constraint assumption (A2) in Eq. (16), thereby completing all aspects of the proof for the stated theorem.

IV. Numerical Simulations

As a test for the control law presented earlier, we consider a representative problem of tracking a rigid body along a commanded trajectory. This commanded motion corresponds to a rotational maneuver starting at rest with the following quaternion vector $\boldsymbol{\beta}^c$ specifying the reference frame with respect to the inertial frame:

$$\boldsymbol{\beta}^c(t) = \sqrt{0.25}\left[0,\ \cos 0.2t,\ \sin 0.2t,\ -\sqrt{3}\right]^T \tag{30}$$

In addition, we impose the control-magnitude and rate constraints at $u_m = 10.0$ and $\dot{u}_m = 5.0$, respectively. The inertia matrix is specified by the matrix

$$I = \begin{bmatrix} 25 & 10 & 5 \\ 10 & 20 & 3 \\ 5 & 3 & 15 \end{bmatrix}$$

At time $t = 0$, the spacecraft orientation is such that the initial attitude described is $\boldsymbol{\beta}(0) = [1, 0, 0, 0]^T$ with a zero initial body angular velocity.

For the particular case of the reference trajectory specified through Eq. (30), we consider the numerical simulation results associated with the controller stated by Eq. (19). As seen from Theorem 1, the gain variables k_p, k_z, and k within Eq. (19) can be selected as any positive constants (values from the first quadrant of the region within the $k_p - k_z$ space) to ensure global asymptotic stability for the closed-loop tracking error dynamics. However, to satisfy the torque and rate constraints, these gain variables need to additionally satisfy the conditions in Eqs. (15) and (16).

The associated control constraint conditions of Eqs. (15) and (16) are plotted in Fig. 1 by using $V_0 = 4u_m$ and the upper bounds of the reference trajectory specified in Eq. (30). In this figure, whereas the torque magnitude constraint given by Eq. (15) manifests as a straight line in the $k_p - k_z$ plane, we also compute and plot the rate-constraint condition of Eq. (16) using three different values for filter gain variable k: (a) $k = 0.25$; (b) $k = 0.5$; and (c) $k = 1.0$. The λ parameter is fixed at a value of 2.0 for each of the three cases for the filter parameter k. Additionally, for the case of $k = 1.0$, the rate constraint condition is evaluated by using $\lambda = 5.0$ to study the effect of increasing λ for the same value of k. It is evident from this figure that choosing $k = 0.25$ implies that the rate-saturation condition is ineffective for the most part in the sense that if we select k_p and k_z values in accordance to the control-magnitude condition alone, then those values would nearly automatically satisfy the rate-saturation condition except within a narrow band of k_p values in the interval (3.5, 5.5). On the other hand, it is also clear from Fig. 1 that choosing $k = 1.0$ dictates that the rate-saturation condition is "active" in the region corresponding to $k_p \in (0, 6.8)$ and the torque magnitude condition takes over the active role for $k_p \ge 6.8$. Thus, we confirm that given particular values for u_m and $\dot{u}_m$, the "feasible" region for $k_p - k_z$ indeed decreases with increasing values of the filter gain k. Another important aspect illustrated in Fig. 1 is that compared to the $\lambda = 2.0$ case, increasing parameter λ to a value of 5.0 while keeping k fixed at 1.0 reduces the feasible region in the $k_p - k_z$ parameter space. Of further significance is the fact that even though the foregoing discussion applies for the particular value of $V_0 = 4u_m$ chosen in these computations (also refer to Remark 2 stated earlier), the qualitative aspect of all observations concerning influence of the filter parameter k remains true for any other choice of $V_0 > 0$.

Once the feasible region for control parameters k_p and k_z is determined, the control design engineer would like to determine specific values for these parameters that would be most desirable in achieving fast convergence for tracking errors. To analyze this aspect, we simulate the closed-loop dynamics with different parameter values chosen from within the feasible region in Fig. 1 to obtain quantitative estimates of time required for convergence of tracking errors. Here, the convergence criterion we adopt is defined by the time t_c

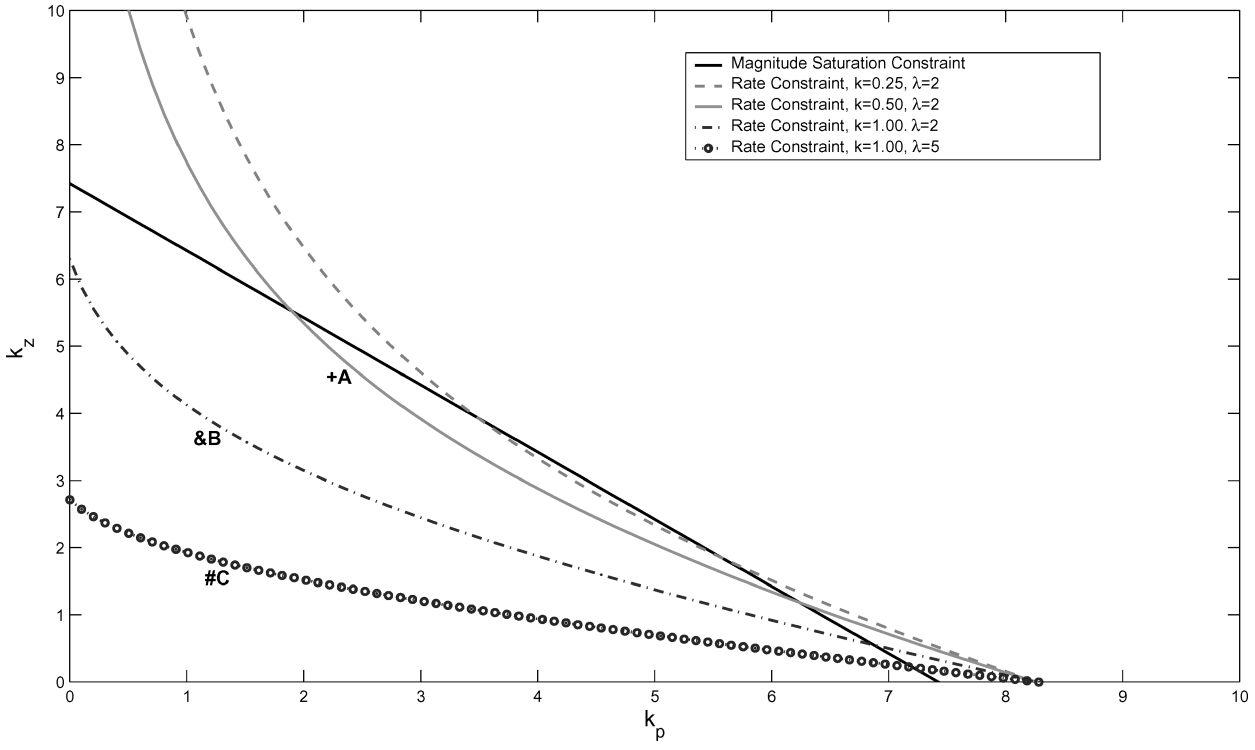

Fig. 1 Torque magnitude and rate constraints in the k_p–k_z parameter space for various values of k and λ.

Table 1 Convergence-time histories for various selections of controller parameters[a]

k_p	$k = 0.25$ $\lambda = 2.0$	$k = 0.5$ $\lambda = 2.0$	$k = 1.0$ $\lambda = 2.0$	$k = 1.0$ $\lambda = 5.0$
0.25	$k_z = 7.1$	$k_z = 7.1$	$k_z = 5.4$	$k_z = 2.4$
	$t_c = 3980$	$t_c = 1016$	$t_c = 445$	$t_c = 445$
0.50	$k_z = 6.8$	$k_z = 6.8$	$k_z = 4.6$	$k_z = 2.2$
	$t_c = 1905$	$t_c = 500$	$t_c = 240$	$t_c = 233$
0.75	$k_z = 6.65$	$k_z = 6.65$	$k_z = 4.4$	$k_z = 2.06$
	$t_c = 1112$	$t_c = 330$	$t_c = 166$	$t_c = 162$
1.0	$k_z = 6.4$	$k_z = 6.4$	$\boldsymbol{k_z = 4.12}$	$k_z = 1.9$
	$t_c = 800$	$t_c = 243$	$\boldsymbol{t_c = 136}$	$t_c = 127$
1.25	$k_z = 6.1$	$k_z = 6.1$	$k_z = 3.8$	$\boldsymbol{k_z = 1.8}$
	$t_c = 620$	$t_c = 190$	$t_c = 144$	$\boldsymbol{t_c = 123}$
1.50	$k_z = 5.9$	$k_z = 5.9$	$k_z = 3.5$	$k_z = 1.7$
	$t_c = 513$	$t_c = 156$	$t_c = 151$	$t_c = 125$
1.75	$k_z = 5.65$	$k_z = 5.65$	$k_z = 3.3$	$k_z = 1.61$
	$t_c = 431$	$t_c = 130$	$t_c = 156$	$t_c = 129$
2.00	$k_z = 5.42$	$k_z = 5.3$	$k_z = 3.14$	$k_z = 1.52$
	$t_c = 365$	$t_c = 110$	$t_c = 161$	$t_c = 137$
2.375	$k_z = 5.0$	$\boldsymbol{k_z = 4.7}$	$k_z = 2.8$	$k_z = 1.39$
	$t_c = 346$	$\boldsymbol{t_c = 100}$	$t_c = 193$	$t_c = 161$
2.50	$k_z = 4.9$	$k_z = 4.41$	$k_z = 2.77$	$k_z = 1.35$
	$t_c = 345$	$t_c = 101$	$t_c = 200$	$t_c = 168$
2.75	$\boldsymbol{k_z = 4.65}$	$k_z = 4.2$	$k_z = 2.6$	$k_z = 1.25$
	$\boldsymbol{t_c = 344}$	$t_c = 109$	$t_c = 215$	$t_c = 183$
3.00	$k_z = 4.4$	$k_z = 3.9$	$k_z = 2.4$	$k_z = 1.2$
	$t_c = 384$	$t_c = 115$	$t_c = 238$	$t_c = 195$
3.5	$k_z = 3.9$	$k_z = 3.3$	$k_z = 2.14$	$k_z = 1.06$
	$t_c = 460$	$t_c = 133$	$t_c = 247$	$t_c = 200$

[a]The fastest convergence-time cases for each k value are indicated in boldface.

taken to reduce $\|\boldsymbol{e}_v(t)\|$ within a value of 10^{-4}. These numerical results are summarized in Table 1.

For each filter parameter k choice, the values of k_p and k_z selected in Table 1 are derived from the outer boundaries of the feasible regions shown in Fig. 1. These choices therefore have the interpretation of being the largest feasible k_z values for corresponding k_p, k, and λ values without violating the actuator magnitude and rate saturation constraints. We note that keeping k fixed (going down each column in Table 1), increase in the k_p parameter leads to decreasing k_z values. In terms of convergence, the rates of tracking error convergence are extremely slow for both small and large values of k_p (respectively large and small values for k_z). Therefore, for each k value, there exists an intermediate value for k_p where the convergence rate is fastest. Ideally, we desire as large a value for k_z (consequently small k_p) as possible in order to make $\dot{V}(t)$ in Eq. (23) as negative as possible. Therefore, k_z may be viewed as a damping coefficient, and large k_z values would correspond to slow convergence rates due to the inherent overdamped nature of the closed-loop dynamics. Similarly, very small k_z values lead to an "underdamped" slow and oscillatory response. There exists an intermediate value for k_z which provides the fastest response for a given choice of parameters k and λ. The numerical results presented in Table 1 confirm this aspect wherein we have highlighted the fastest convergence time cases for each k value in bold font.

In terms of tracking error convergence rates, the data presented in Table 1 indicates that while using $k = 0.25$, the fastest convergence $t_c = 344$ occurs when $(k_p, k_z, \lambda) = (2.75, 4.65, 2.0)$. However, this rate of convergence is very slow compared to the best convergence rate of $t_c = 100$ obtained using $(k, k_p, k_z, \lambda) = (0.5, 2.375, 4.7, 2.0)$. On the other hand, further increase in the value of k provides a best $t_c = 136$, which is again slow compared to the fastest t_c obtained using $k = 0.5$. Therefore, from the point of view of convergence rates, there exists an optimal value for the filter parameter k that provides fastest tracking error decay rates. Another interesting aspect evident from Table 1 is that keeping k fixed at any particular value ($k = 1$ in this case), the convergence rates can be moderately accelerated by using a larger λ value. Of course, larger λ invariably causes higher torque rates, thereby "shrinking" the feasibility region in the $k_p - k_z$ parameter space (refer to Remark 5 stated earlier).

The closed-loop tracking errors as a consequence of our choice of $(k, k_p, k_z, \lambda) = (0.5, 2.375, 4.7, 2.0)$ within the control law described by Eq. (19) are shown in Fig. 2. These gain parameters correspond to the "+A" point in the $k_p - k_z$ feasibility space shown in Fig. 1. The corresponding control torques given by $\boldsymbol{u}(t)$ and the control-rate signals are also shown in Fig. 2. It is to be noted from the plots that the proposed control law satisfies the magnitude constraint on the torque ($\max(\|\boldsymbol{u}(t)\|) \approx 4.0 \leq u_m$) and its rate ($\max(\|\dot{\boldsymbol{u}}(t)\|) \approx 3.0 \leq \dot{u}_m$) well within the bounds we have specified. The tracking errors $\boldsymbol{\delta\omega}(t)$ and $\boldsymbol{e}(t)$ achieve convergence after about 100 s of simulation, which is also consistent with the results tabulated in Table 1. The effects of sensor noise are not included in this simulation.

Our next simulation considers the presence of noise in the sensor outputs. Corresponding to the same simulation case considered earlier with $(k, k_p, k_z, \lambda) = (0.5, 2.375, 4.7, 2.0)$, we include zero-mean noise signal having a moderate standard deviation of 0.03 within each component of the error quaternion $[\boldsymbol{e}_v, e_0]^T$. It could be noted that a standard deviation of 0.03 on quaternion measurements physically corresponds to about 4 degrees error in the Euler angles (say, a 3–2–1 rotation sequence). Therefore, our simulations correspond to the adoption of a very coarse attitude sensor when compared to the noise-corrupted simulation results of velocity-free attitude controllers presented in Ref. 8. The noise-corrupted quaternion signal is renormalized to make it a unit vector and implemented within the feedback torque commanded by Eq. (19). The closed-loop dynamics are simulated to study the performance of the velocity-free control structure with respect to sensor noise effects. These results are shown in Fig. 3. The tracking errors reported in this figure show that good performance can indeed be obtained through the velocity-free control structure in the presence of sensor noise. Importantly, the effects of noise are not being unacceptably amplified because of the adoption of the filter dynamics governed by Eq. (18).

To further investigate the role played by the value of the filter parameter k on noisy measurements, we consider two distinct cases: 1) parameter choice "+A" designated in Fig. 1, described by $k = 0.5$, $(k_p, k_z, \lambda) = (2.375, 4.7, 2.0)$; and 2) choice "&B" shown in Fig. 1 using $k = 1.0$, $(k_p, k_z, \lambda) = (1.0, 4.12, 2.0)$. For each of these two cases, we perform numerical simulations including the effects of sensor noise. The levels of sensor noise added in both cases are the same, having zero mean with a standard deviation of 0.03. The standard deviations of the three components of the control-torque vector are computed to study how the value of k impacts the overall noise levels within the closed-loop simulation. These results are summarized in Table 2. The standard deviation of the jth torque component is designated as σ_u^j for $j = 1, 2, 3$. As expected in Remark 6, the simulation data confirm that adopting a higher value for the filter parameter k as in case 2) provides for an overall reduction in the noise levels when compared to the relatively smaller k value in case 1). At the same time, it may also be noted from Table 1 that the larger k value case &B takes a longer convergence time of $t_c = 136$ when compared to the smaller k value in +A where $t_c = 100$. Therefore, we have an important trade-off that arises from the practical considerations of sensor noise rejection vis-à-vis desire for faster tracking error convergence. If faster convergence is the sole design criterion, then one can determine an optimal value for the filter parameter k, which may, however, exhibit inferior sensor-noise-rejection properties. On the other hand, the effects of noisy measurements on the control torques can be greatly reduced by using larger and larger values for the filter parameter k. In this case, the penalty comes through lower tracking-error-convergence rates. In this context, the additional degree of freedom available through

Table 2 Simulation data comparing the noise levels in the control torque as impacted by the choice of different filter parameter k values

Parameter values from Fig. 1	σ_u^1	σ_u^2	σ_u^3
"+A": $k = 0.5$	0.0781	0.0754	0.0788
"&B": $k = 1.0$	0.0587	0.0546	0.0600

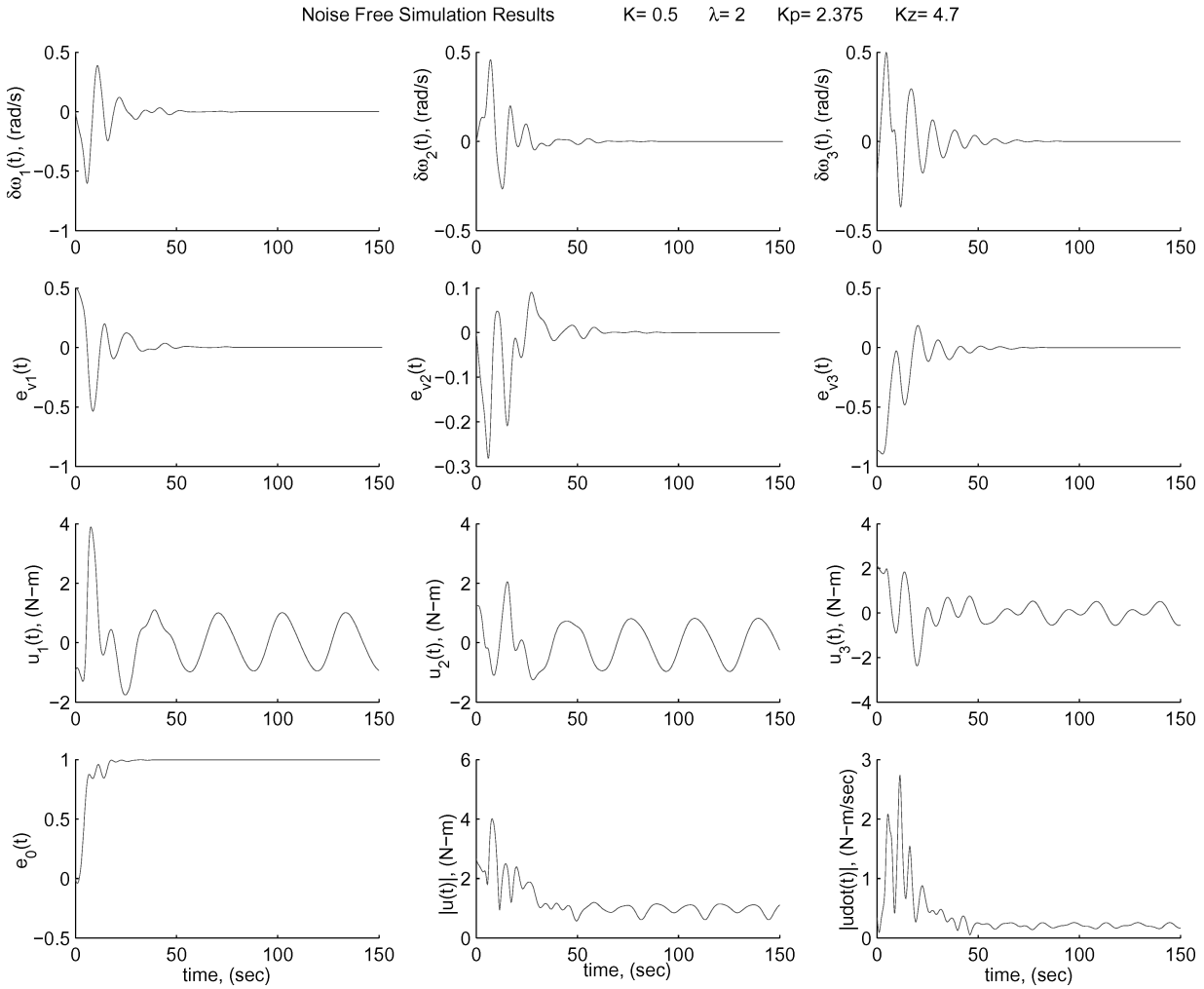

Fig. 2 Numerical simulations for noise-free case.

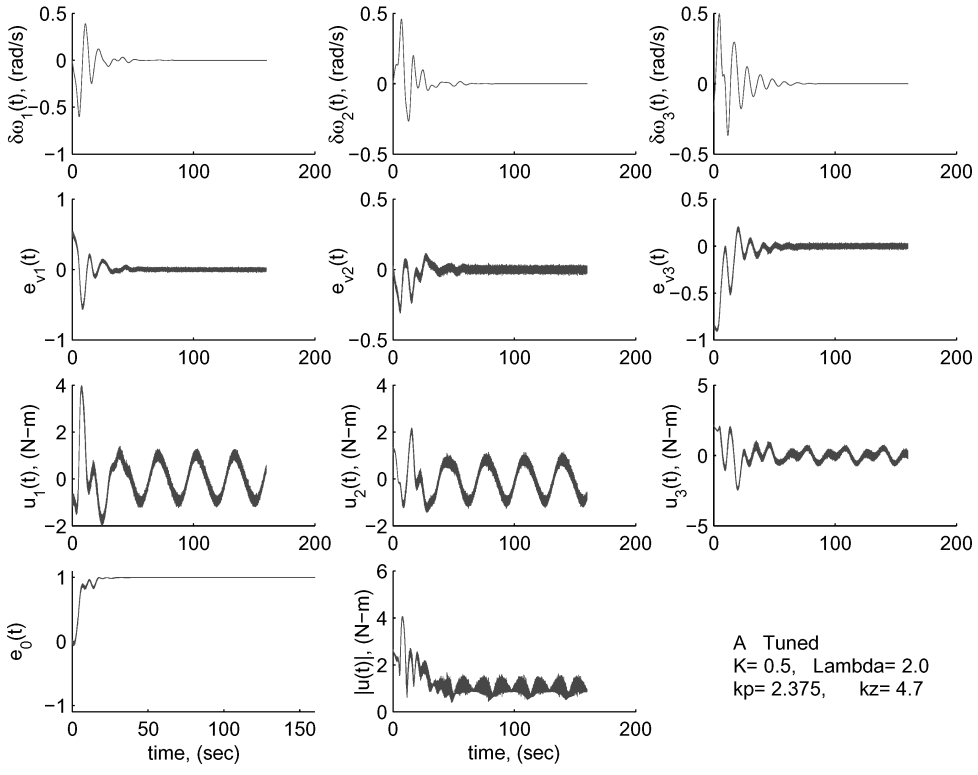

Fig. 3 Numerical simulations including noise.

the proposed control structure in terms of the parameter λ can help in improving the convergence speeds even when higher k values are utilized. This flexibility in having the ability to tune the parameter λ in order to achieve larger values for the filter parameter k without much sacrifice in the tracking error convergence rates may be construed as a distinct advantage of the control torque, Eq. (19), provided by Theorem 1.

V. Conclusions

In this paper, we consider the passivity-based output feedback control problem associated with attitude tracking of a rigid body subject to actuator saturation. In this context, output feedback implies that only the attitude measurement is available for feedback and the body angular-velocity vector is not employed in the synthesis of smooth and differentiator-free control algorithms. When compared to the standard problem of output feedback attitude control without control saturations, the proposed control scheme requires availability of additional a priori information (an upper bound on the norm of the initial angular velocity and upper bounds on the signals defining the reference trajectories). The kinematic part of the governing equations is expressed in terms of the four-dimensional quaternion vector. This choice for the kinematics and our adoption of hyperbolic tangent functions play crucial roles in enabling our formulation. The control solution derived here guarantees asymptotic stability for tracking-error dynamics about all bounded reference trajectories in the presence of control magnitude and rate saturation constraints. Our control solution utilizes the passivity filter variable synthesized through a first-order stable differential equation that is parameterized in terms of a filter parameter k and is forced by the attitude error vector (measurement). In the practical case where there exists noise in the measurement of the attitude variable, it is always desirable to utilize as large a value for the filter parameter k as permitted within the control saturation bounds. In this context, we have demonstrated through both analysis and numerical simulations that the hyperbolic trignometric functions present within our new construction impart greater flexibility for tuning the controller through the presence of the λ parameter. This benefit is evident from the fact that relatively large values can be utilized for the filter parameter k without compromising either control smoothness or asymptotic convergence rates (closed-loop performance) for the tracking errors.

Acknowledgments

These results are based in part on work supported by the Texas Advanced Research Program under Grant 003658-0081-2001. The manuscript is the revised version of a paper that was originally presented at the Fourteenth U.S. National Congress of Theoretical and Applied Mechanics, Blacksburg, Virginia, 23–28 June 2002. We thank the Associate Editor and the anonymous reviewers for all of their insightful remarks.

References

[1]Wen, J., and Kreutz-Delgado, K., "The Attitude Control Problem," *IEEE Transactions on Automatic Control*, Vol. AC-36, No. 10, 1991, pp. 1148–1162.

[2]Wie, B., Weiss, H., and Arapostathis, A., "Quaternion Feedback Regulator Spacecraft Eigenaxis Rotations," *Journal of Guidance, Control, and Dynamics*, Vol. 12, No. 3, 1989, pp. 375–380.

[3]Junkins, J. L., Akella, M. R., and Robinett, R. D., "Nonlinear Adaptive Control of Spacecraft Maneuvers," *Journal of Guidance, Control, and Dynamics*, Vol. 20, No. 6, 1997, pp. 1104–1110.

[4]Paielli, R. A., and Bach, R. E., "Attitude Control with Realization of Linear Error Dynamics," *Journal of Guidance, Control, and Dynamics*, Vol. 16, No. 1, 1993, pp. 182–189.

[5]Schaub, H., Akella, M. R., and Junkins, J., "Adaptive Realization of Linear Closed Loop Tracking Dynamics in the Presence of Large System Model Errors," *Journal of Guidance, Control, and Dynamics*, Vol. 23, No. 5, 2000, pp. 95–100.

[6]Lizarralde, F., and Wen, J. T., "Attitude Control Without Angular Velocity Measurement: A Passivity Approach," *IEEE Transactions on Automatic Control*, Vol. AC-41, No. 3, 1996, pp. 468–472.

[7]Tsiotras, P., "Further Passivity Results for the Attitude Control Problem," *IEEE Transactions on Automatic Control*, Vol. AC-43, No. 11, 1998, pp. 1597–1600.

[8]Caccavale, F., and Villani, L., "Output Feedback Control for Attitude Tracking," *Systems and Control Letters*, Vol. 38, No. 2, 1999, pp. 91–98.

[9]Akella, M. R., "Rigid Body Attitude Tracking Without Angular Velocity Feedback," *Systems and Control Letters*, Vol. 42, No. 4, 2001, pp. 321–326.

[10]Teel, A. R., and Praly, L., "Tools for Semiglobal Stabilization by Partial State and Output Feedback," *SIAM Journal of Control and Optimizations*, Vol. 33, No. 5, 1995, pp. 1443–1488.

[11]Esfandiari, F., and Khalil, H. K., "Output Feedback Stabilization of Fully Linearizable Systems," *International Journal of Control*, Vol. 56, No. 5, 1992, pp. 1007–1037.

[12]Schaub, H., Robinett, R. D., and Junkins, J. L., "New Penalty Functions for Optimal Control Formulation for Spacecraft Attitude Control Problems," *Journal of Guidance, Control, and Dynamics*, Vol. 20, No. 3, 1997, pp. 428–434.

[13]Loria, A., and Nijmeijer, H., "Bounded Output Feedback Tracking Control of Fully Actuated Euler–Lagrange Systems," *Systems and Control Letters*, Vol. 33, No. 3, 1998, pp. 151–161.

[14]Stanley, W. S., "Quaternion from Rotation Matrix," *Journal of Guidance and Control*, Vol. I, No. 3, 1978, pp. 223, 224.

[15]Shuster, M. D., "A Survey of Attitude Representations," *Journal of the Astronautical Sciences*, Vol. 41, No. 4, 1993, pp. 439–517.

[16]Ioannou, P. A., and Sun, J., *Stable and Robust Adaptive Control*, Prentice–Hall, Upper Saddle River, NJ, 1995, pp. 76, 77.

[17]Junkins, J. L., and Turner, J. D., *Optimal Spacecraft Rotational Maneuvers*, Elsevier, Amsterdam, 1986, pp. 12–14.